Turbulence Characteristics behind a Flexible Vortex Generator

SHARUL SHAM DOL
Department of Mechanical Engineering
Abu Dhabi University
Abu Dhabi, P.O. Box 59911
UNITED ARAB EMIRATES
sharulshambin.dol@adu.ac.ae

CHAN HIANG BIN
Department of Mechanical Engineering
Curtin University Malaysia
CDT 250, 98009 Miri Sarawak
MALAYSIA
hiang.bin@postgrad.curtin.edu.my

WEE SIAW KHUR
Department of Mechanical Engineering
Curtin University Malaysia
CDT 250, 98009 Miri Sarawak
MALAYSIA
wee.siaw.khur@curtin.edu.my

PERUMAL KUMAR
Department of Chemical Engineering
Curtin University Malaysia
CDT 250, 98009 Miri Sarawak
MALAYSIA
p.kumar@curtin.edu.my

Abstract: - This paper computationally studied the turbulence characteristics of the wake behind a free-oscillating flexible vortex generator (FVG) by investigating the shear rate around the FVG using Fluid-Structural Interaction (FSI) simulation of RANS (SST) *k-w* model. Two vortex generators are considered in this study; a circular and a flat plate cantilever. Each vortex generator was submerged individually in a sub-critical flow ($10^2<Re<10^5$). Firstly, the wall shear stress generated by the FVG was found to be greater than the rigid vortex generator (RVG), which denotes that the turbulence source has become stronger when a FVG is implemented. The time-series of the wall shear stress was investigated and it was observed that the maximum wall shear stress occurred when the FVG was in motion whilst the minimum wall shear stress occurred when the FVG stopped moving. The proposed flow model suggests that the increasing wall shear stress is scaled with the structural velocity. Secondly, the vortex strength was analyzed. It was found that the FVG is capable of generating stronger vortices compared to the RVG; which in other words, the FVG has a better turbulence generation ability due to the stronger turbulence production at the boundary layer, hence better energy mixing for heat transfer enhancement.

Key-Words: - downwash, mixing, production term, shear stress, turbulence, URANS, vortex generator

1 Introduction

This study proposes a strategy to enhance the vortex generator's (VG) turbulence generation ability via amplifying the VG's flexibility, hence creating a flexible vortex generator (FVG). Unlike the rigid vortex generator (RVG) that is static, the enhanced flexibility of the FVG allows it to oscillate as it responds to the flow, resulting in a more dynamical interaction with the flow. As a result, a more chaotic flow is anticipated.

The study of flow dynamics behind an oscillating object is uncommon, although the structural dynamics of a similar setup has been studied extensively, most notably on the lock-in effect. Despite being out of the spotlight, the studies of vortex pattern behind oscillating object, in both 2-dimensional and 3-dimensional settings, receive a slightly better attention compared to other aspects of its flow dynamics. All observations reported in the literature [1-5] are consistent with the vortex pattern map founded by William and Roshko [6].

The turbulence characteristics, on the other hand, has received less attention. Griffin [7] analysed the velocity fluctuation at the wake of a forced-oscillating cylinder and found that it was greater than a stationary cylinder; signifying greater turbulence. However, the oscillation was induced actively through external energy supply, which might not be able to provide useful insight to the current work that focuses on a passively oscillating object.

The next relevant study was published 30 years after Griffin's work, by Gorvadhan and Williamson [8], who studied the velocity field behind an elastically-mounted cylinder (rigid cylinder mounted with springs to allow passive oscillation) via Particle Image Velocimetry (PIV) measurements. They computed and compared the Reynolds stresses and found that it is approximately 100% to 485% greater

behind a passively-oscillating cylinder compared to the stationary one. This implies that the oscillating cylinder had generated greater turbulence.

Ali et al. [9] conducted a numerical study on a concept similar to the current study. They simulated the flow in a channel with a series of tilted flexible winglets located at the wall. Coincidently, they also named the winglets as flexible vortex generators (FVGs). Their study focused on the mixing quality by analysing the transport a passive scalar. They found that the FVGs had achieved 97%~98% better mixing compared to the rigid case with the same configuration and flow condition.

Yong et al. [10] conducted a series of experiments investigating the performance of flexible finite cylinder – similar to the current research focus. The velocity field was measured and the turbulence production term ($-\overline{u'_i u'_j} \cdot \partial U_i / \partial x_j$) was computed. They credited the weakening of downwash (observed from the diminishing vertical velocity component) as the cause of such enhancement.

This work plans to investigate the role of flexible cantilever as a FVG in turbulence generation with respect to RVG. More importantly, the present work also plans to explore the underlying physics behind the turbulence enhancement achieved by the FVG, which is still an unanswered question in the current understanding. Therefore, instead of analysing the fluctuation field that could only provide a statistical description of turbulence, the shear component of the flow is examined to shed light on the physics.

2 Numerical Model

After reviewing some related studies, it is found that the RANS model is one of the popular fluid flow models that has been used in simulating the FSI simulation [11-17].

2.1 Fluid flow model

Unsteady Reynolds-Averaged Navier-Stokes (URANS) equation is used to compute the fluid flow. (SST) *k-ω* turbulence model is used to model the turbulence. Equation (1) is the URANS equation and equation (2) represents the continuity equation in the URANS formulation.

$$\rho\left[\frac{\partial U_i}{\partial t}+U_j\frac{\partial U_i}{\partial x_j}\right]=-\frac{\partial P}{\partial x_i}+\rho g_i + \frac{\partial}{\partial x_j}\left[\mu\frac{\partial U_i}{\partial x_j}-\rho\overline{u'_i u'_j}\right]+S_{m,i} \quad (1)$$

$$\frac{\partial U_i}{\partial x_i}=0 \quad (2)$$

Equation (3) denotes the energy equation and (4) is the equation of specific dissipation that are used in the (SST) *k-ω* turbulence model.

$$\frac{\partial k}{\partial t}+u_i\frac{\partial k}{\partial x_j}=P_k-\beta^* k\omega+\frac{\partial}{\partial x_j}\left((\nu+\sigma_k\nu_\tau)\frac{\partial k}{\partial x_j}\right) \quad (3)$$

$$\frac{\partial \omega}{\partial t}+u_i\frac{\partial \omega}{\partial x_j}=\alpha S^2-\beta\omega^2+\frac{\partial}{\partial x_j}\left((\nu+\sigma_k\ \nu_\tau)\frac{\partial \omega}{\partial x_j}\right)+2(1-F_1)\sigma_{\omega 2}\frac{1}{\omega}\frac{\partial k}{\partial x_i}\frac{\partial \omega}{\partial x_i} \quad (4)$$

2.2 Structural model

The typical (3 degree-of-freedom) equation of motion (equation 5) is used to model the structural motion.

$$m\ddot{x}+q\dot{x}+kx=\sum F_x \quad (5)$$

where F_i is the force in *i*-direction, *m* is the mass, *q* is the damping coefficient and *k* is the spring constant.

2.3 Coupling method

In the present work, a strong two-way FSI coupling method is used. Besides, an implicit coupling scheme is used during data transfer.

2.4 Domain and boundary conditions

Figure 1 represents the simulation domain used in this study. Uniform flow was applied to the inlet of the domain. The boundary conditions of the flow domain are summarized in Table 1. In this study, the circular and flat plate cantilever are used as the VG. Besides, it is important to note that the purpose of studying two geometries is to extract more information about its behaviours and physics that could be concealed if only one geometry is studied [18]. The fluid, flow and structural properties of the simulated cases are tabulated in Table 2.

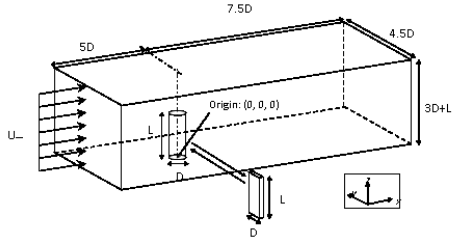

Fig. 1. Schematic of the fluid domain (not to scale).

Table 1. List of boundary conditions

Surface	Boundary type
Inlet	Velocity Inlet
Outlet	Pressure Outlet
Bottom surface	Non-Slip Wall
Cylinder	Non-Slip Wall; Co-simulation Interface (flexible)
Top surface	Symmetry Plane
Side surfaces	Symmetry Plane

Table 2 The fluid, flow and structural properties used in the circular and flat plate VGs simulation

Fluid Properties	Circular Case	Flat Plate Case
Fluid	Water	Air @20˚C
Density	998.2 kg/m^3	1.1842 kg/m^3
Dynamic viscosity	1.002×10^{-3} Pa·s	1.855×10^{-5} Pa·s
Flow Properties		
Reynolds Number	~3500	~11500
Inlet Velocity	0.35 m/s	4.5 m/s
Inlet Turbulence Intensity	0.5%	0.5%
Structural (VG) Properties		
Cross-sectional geometry	Circular	Thin Flat Plate
Characteristic length	Diameter=0.01m	Width=0.04m Thickness=0.002m
Aspect Ratio	6, 8 and 10	4, 5 and 6
Second Moment of Inertia	4.91×10^{-10} m^4	2.67×10^{-11} m^4
Material	Silicon Foam	Teflon
Young's Modulus	486927 Pa	5.0×10^{-8} Pa
Density	676.78 kg/m^3	2200 kg/m^3
Poisson ratio	0.4	0.46

2.5 Mesh independence study

Mesh independence study was conducted to obtain the best mesh. The $y+$ value was constantly monitored (according to the Law of Wall, $y+ \leq 5$ is required) to ensure the near wall meshes model the boundary layer correctly. An unstructured polyhedral mesh is used to mesh the domain. The details of meshes used in this study are tabulated in Table 3. The drag coefficient, pressure profile and velocity profile were monitored to get the optimal mesh size, as shown in Fig. 2.

Based on the study, Mesh 4 is found to be the optimum mesh setting, selected based on the convergences of each monitored data, as the mesh size was refined. The result shows that any further refinement from Mesh 4 to Mesh 5 does not result in significant differences. The meshes of the circular and flat plate cantilevers are as shown in Fig. 3. A structured hexahedral mesh is used on the VGs.

Table 3 Summary of meshes and its respective information

Mesh No.	Targeted Max. Mesh Size	Targeted Min. Mesh Size	Cylinder Surface Mesh	Number of Cells	Obtained Max. $y+$
Mesh 1	0.6D	0.150D	0.150D	136979	3.63
Mesh 2	0.5D	0.125D	0.125D	149176	3.58
Mesh 3	0.4D	0.100D	0.100D	306901	3.34
Mesh 4	0.3D	0.075D	0.075D	543050	3.63
Mesh 5	0.2D	0.050D	0.050D	1573239	3.71

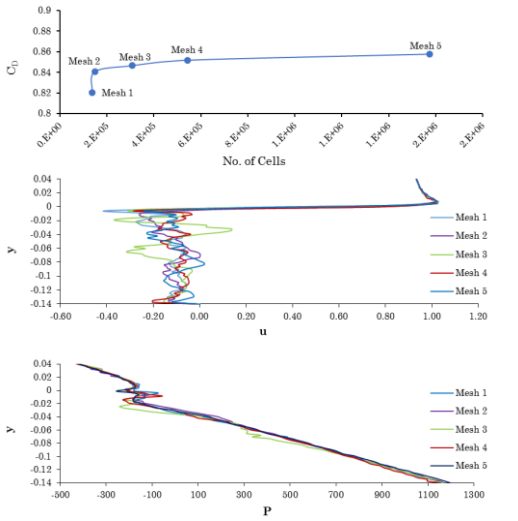

Fig. 2. The mesh independency study: (i) drag coefficient, (ii) pressure profile at x/D=0.75 downstream and (iii) velocity profile x/D=0.75 downstream.

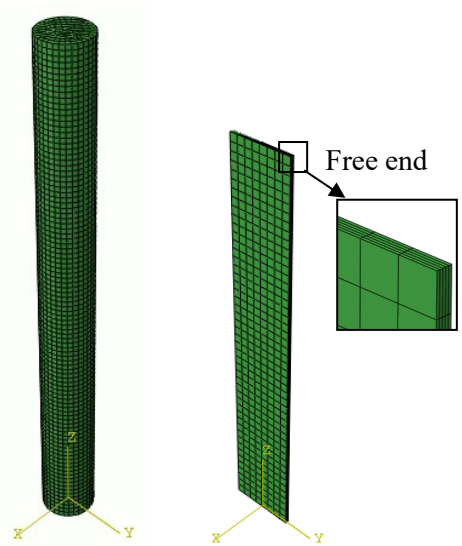

Fig. 3. The structured hexahedral mesh on the circular and flat plate VGs.

2.6 Model's physics validation

Since the current work analyzes the shear of mean flow, the mean flow field needs to be correctly simulated. This aspect was validated by reproducing the velocity profile behind a cantilever, experimentally measured by Okamoto and Yagita [19]. The comparison, as shown in Fig. 4, shows that the simulated result matches well with the experimental data;

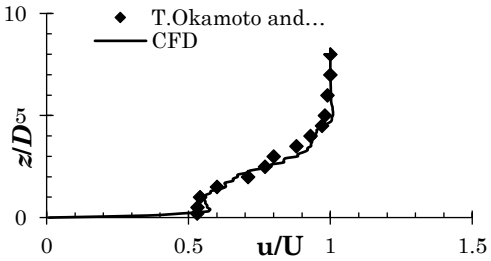

Fig. 4. The velocity profile validation with Okamoto and Yagita [19].

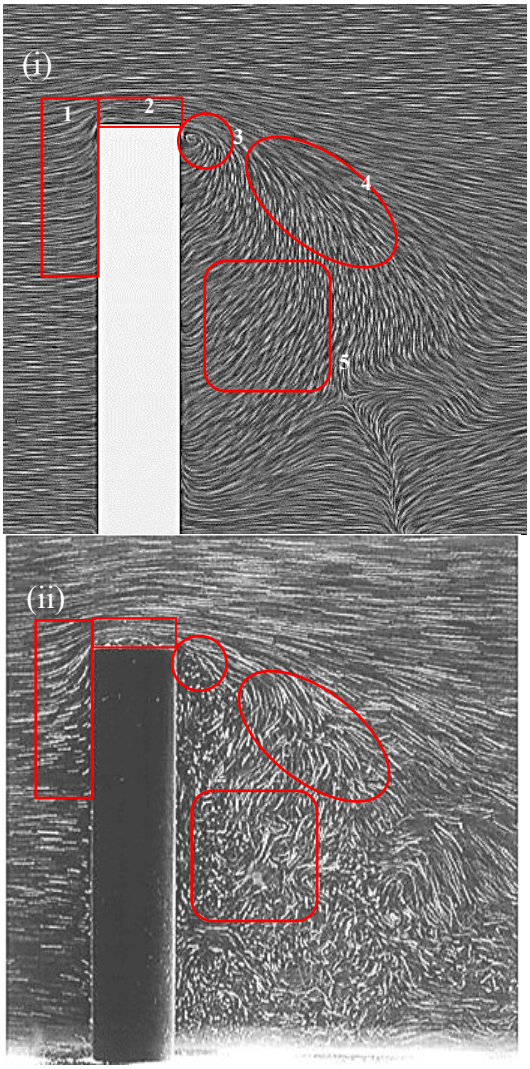

Fig. 5. Flow field comparison: (i) CFD – Mesh 4 and (ii) experimental visualization captured by Park and Lee [20].

The unique flow features, such as downwash and upwash, generated by the cantilever is also one of the main key aspects that must be validated. This validation was done by reproducing the flow field that was visualized by Park and Lee [20]. According to the comparison shown in Fig. 5, the key features such as the upwash, downwash, recirculation zone and the mean flow direction have been reproduced with a good degree of agreement.

Lastly, the coupling between the CFD and FEA to simulate a FSI problem was also validated by reproducing one of the benchmarks introduced by Tian et al. [21]. In this validation, a flexible flat plate cantilever submerged perpendicularly to a flow was simulated. The validation results are summarized in Table 4.

Table 4 The comparison of the current model with the benchmark from Tian *et al.* [21]

	C_D	Force (N)	Normalized *x*-displacement (*x*/*D*)
CFD	1.19	0.00645	2.53
Tian *et al.* (2014)	0.94	0.00616	2.45
Error (%)	n/a	4.7%	4.1%

3 Results and Discussions

Shear plays an important role in turbulent flow. According to the Kinetic Budget Equations, the bulk flow regime loses its energy to the turbulent regime. Then, the turbulent regime uses this energy to sustain the turbulence. This energy gained by the turbulent regime is known as the shear production or turbulence production in the budget equations, as shown in Eq. (6).

$$\pm \overline{u'_i u'_j} \frac{\partial U_i}{\partial x_j} \qquad (6)$$

The expression shows that the shear production is governed by two aspects, namely the Reynolds stresses ($\overline{u'_i u'_j}$) and the shear rate ($\frac{\partial U_i}{\partial x_j}$). The present work will be focusing on the modification of shear rate when the FVG is used. Two shear rates will be examined in this work, namely the wall shear stress and the circulation. The detail of each shear rate will be discussed later.

Besides, an abbreviation will be introduced to facilitate the following discussion. With this abbreviation, the lengthy "AR=8 circular FVG" can be written as 8_{CF} accordingly; where the "8" denotes the aspect ratio, the subscript "$_C$" denotes "circular" (it will be "$_P$" for flat plate), and the "$_F$" denotes "FVG" (it will be "$_R$" for RVG). Using this concept, "AR=5 flat plate RVG" can be written as 5_{PR}.

The wall shear stress is the most straightforward variable that displays the characteristic of shear rate, as shown by Eq. (7).

$$\tau_{w,i} = \mu \frac{\partial U_i}{\partial x_j} \quad (7)$$

According to the equation, the τw is the product of the dynamic viscosity and the shear rate. Since the dynamic viscosity is constant for an incompressible fluid, the τ_w can directly reflect any modifications or changes of shear rate. The wall shear stress of a circular case and flat plate case are shown in Fig. 6 and Fig. 7, respectively.

Firstly, from the comparison between the τ_w on the RVG and FVG, it shows the τ_w on the FVG is generally greater than that on the RVG: it increased 9.3%~75.0% for circular case and 5.0%~66.7% for flat plate case, where the greater increment is observed near the FVG's free end (the location with greater oscillation amplitude) and the weaker increment is seen near the FVG's root (the location with small or no oscillation amplitude). To identify the cause of this escalation in the FVG case, the evolution of τ_w (the time-series) on the circular FVG was studied, as shown in Fig. 8. The result clearly shows that high magnitude of the τ_w is present when the FVG is in motion. Conversely, the low magnitude of the τw is observed at the moment when the FVG has attained its maximum deflection, i.e. the FVG stops moving at this point. A similar result and behavior are displayed by the flat plate FVG.

This result strongly suggests that the increment of the wall shear stress magnitude is resulted by the oscillation or the motion of the FVG. A flow model is proposed to theoretically explain this phenomenon via relating the FVG's motion with the formation of velocity gradient on the structure's surface, as shown in Fig. 9. It is important to note that the structure's surface is assumed a non-slip wall. According to the model, a non-zero velocity is formed at the wall of the moving structure, where its sign is depending on the direction of the structure's motion. In the case when it moves against the flow, a negative flow velocity is formed at the wall, which drastically increases the velocity gradient near the wall, as shown in the figure. As a result, the τ_w on a moving structure (such as the FVG) appears to be greater than a stationary one. Apart from this, the model also shows that the escalation of the τ_w scales with the structural velocity (U_s): a greater U_s can lead to a greater τ_w, or vice versa. This prediction will be examined shortly to validated the proposed flow model.

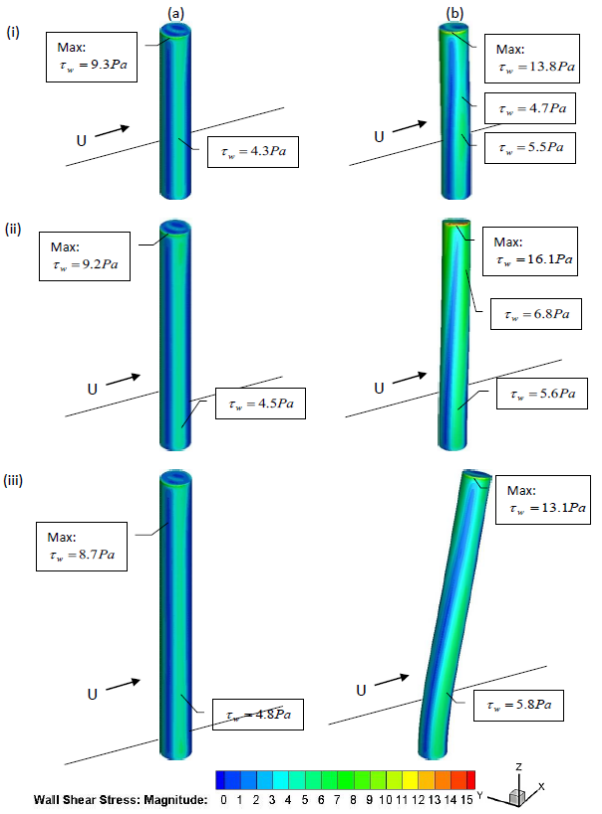

Fig. 6. Instantaneous wall shear stress magnitude (Pa) contour on the circular (a) RVG and (b) FVG with (i) AR=6, (ii) AR=8 and (iii) AR=10

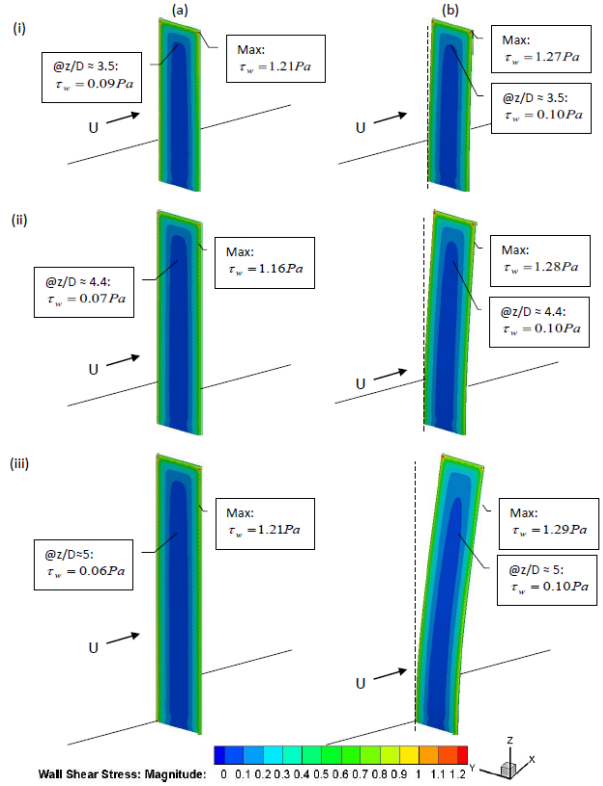

Fig. 7. Instantaneous wall shear stress magnitude (Pa) contour on the flat plate (a) RVG and (b) FVG with (i) AR=4, (ii) AR=5 and (iii) AR=6

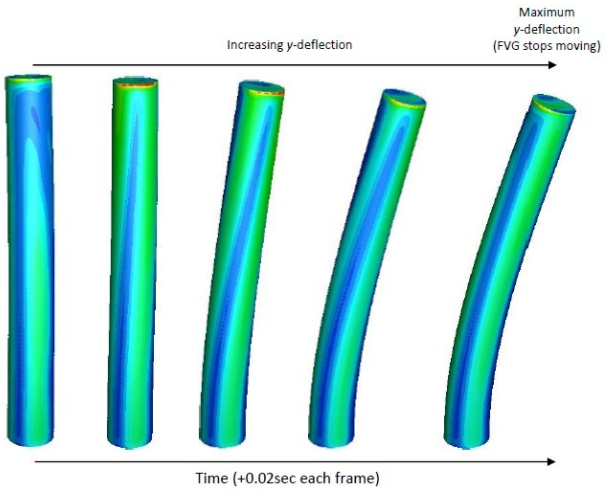

Fig. 8. The change of wall shear stress contour on an AR=8 circular FVG as it is deflecting

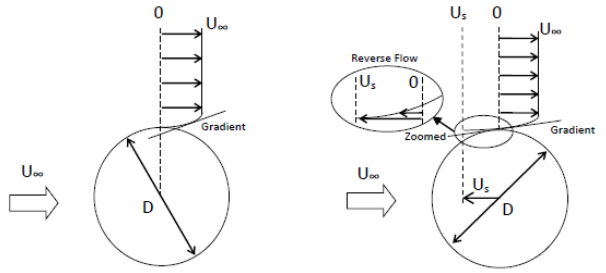

Fig. 9. Velocity gradient on the surface of a submerged structure: (left) stationary (right) moving against the flow with velocity U_s

In general, the FVG can also generate wake with greater height compared to the RVG. In the current study, the circular FVGs have generated wake with 25.0~62.2% taller wake than the wake of the RVG; and the flat plate FVGs' wake is at most ~21.3% taller than the wake of the RVG. The wake height increment is caused by the weakening or vanishing of downwash behind the FVG. The weakening or vanishing of downwash is scaled with the degree of deflection; the greater the deflection, the weaker the downwash. The width of the wake does not differ significantly despite a large transverse motion (along the axis where the width is measured) of the FVG.

Since the wake represents the effective region where turbulence activities can take place, a larger wake generated by the FVGs denotes a spatially greater turbulence compared to the RVGs. Besides, this present study has demonstrated a different angle to study turbulence generation ability other than the classical statistical study. The spatial analysis shed light on the possibility to actively control the spatial scale of turbulence [22], without compromising the turbulence strength, by simply altering the deflection of a VG in the system.

5 Conclusion

Turbulence is a very useful flow characteristic that is used in many engineering devices to facilitate mixing and/or heat transfer. Based on the results, it can be concluded that the FVG has a better turbulence generation ability compared to its respective rigid counterpart. The physics of this phenomenon is also identified. The author noticed that the proposed flow model can potentially provide a universal explanation to any similar phenomenon (i.e. vortex strength, turbulence generation, shear layer physics) for any submerged structure (with any geometry and shape) that is in motions, including rotational motion. The potential of the flow model, thus, should be further explored.

References:

[1] Zahari, M. A., and S. S. Dol. "Application of vortex induced vibration energy generation technologies to the offshore oil and gas platform: The preliminary study." *International Journal of World Academy of Science, Engineering and Technology*8.7 (2014): 1331-34.

[2] Zahari, M. A., and S. S. Dol. "Effects of Different Sizes of Cylinder Diameter on Vortex-Induced Vibration for Energy Generation." *Journal of Applied Sciences* 15.5 (2015): 783-791.

[3] Fujarra, A. L. C., C. P. Pesce, F. Flemming, and C. H. K. Williamson. "Vortex-induced vibration of a flexible cantilever." *Journal of Fluids and Structures* 15, no. 3 (2001): 651-658.

[4] Yamamoto, C. T., J. R. Meneghini, F. Saltara, R. A. Fregonesi, and J. A. Ferrari. "Numerical simulations of vortex-induced vibration on flexible cylinders." *Journal of fluids and structures* 19, no. 4 (2004): 467-489.

[5] Lam, K. M., P. Liu, and J. C. Hu. "Combined action of transverse oscillations and uniform cross-flow on vortex formation and pattern of a circular cylinder."*Journal of Fluids and Structures* 26, no. 5 (2010): 703-721.

[6] Williamson, C. H. K., and A. Roshko. "Vortex formation in the wake of an oscillating cylinder." *Journal of fluids and structures* 2, no. 4 (1988): 355-381.

[7] Griffin, Owen M. "The unsteady wake of an oscillating cylinder at low Reynolds

number." *Journal of Applied Mechanics* 38, no. 4 (1971): 729-738.

[8] Govardhan, R., and C. H. K. Williamson. "Mean and fluctuating velocity fields in the wake of a freely-vibrating cylinder." *Journal of Fluids and Structures* 15, no. 3 (2001): 489-501.

[9] Ali, S., C. Habchi, S. Menanteau, T. Lemenand, and J. Harion. "Heat transfer and mixing enhancement by free elastic flaps oscillation." *International Journal of Heat and Mass Transfer* 85 (2015): 250-264.

[10] Yong, T. H., H. B. Chan, S. S. Dol, S. K. Wee, and P. Kumar. "The flow dynamics behind a flexible finite cylinder as a flexible agitator." *IOP Conference Series: Materials Science and Engineering*, 206 (2017). DOI: 10.1088/1757-899X/206/1/012033.

[11] Constantinides, Y. and O. H. Oakley. "Numerical prediction of bare and straked cylinder VIV*." OMAE2006-92334* (2006).

[12] Huang, Z. Y., Z. Y. Pan, and W. C. Cui. "Numerical simulation of VIV of a circular cylinder with two degrees of freedom and low mass-ratio." *Journal of ship mechanics* 11, no. 1 (2007): 1.

[13] Willden, R. H. J., and J. M. R. Graham. "Numerical prediction of VIV on long flexible circular cylinders." *Journal of Fluids and Structures* 15, no. 3 (2001): 659-669.

[14] Pan, Z. Y., W. C. Cui, and Q. M. Miao. "Numerical simulation of vortex-induced vibration of a circular cylinder at low mass-damping using RANS code." *Journal of Fluids and Structures* 23, no. 1 (2007): 23-37. https://doi.org/10.1016/j.jfluidstructs.2006.07.007

[15] Guilmineau, E., and P. Queutey. "Numerical simulation of vortex-induced vibration of a circular cylinder with low mass-damping in a turbulent flow." *Journal of fluids and structures* 19, no. 4 (2004): 449-466.

[16] Zhao, M., and L. Cheng. "Numerical investigation of local scour below a vibrating pipeline under steady currents." *Coastal Engineering* 57, no. 4 (2010): 397-406.

[17] Ding, L., M. M. Bernitsas, and E. S. Kim. "2-D URANS vs. experiments of flow induced motions of two circular cylinders in tandem with passive turbulence control for 30,000< Re< 105,000." *Ocean Engineering* 72 (2013): 429-440.

[18] Chan, H. B., T. H. Yong, P. Kumar, S. K. Wee, and S. S. Dol. "The numerical investigation on the effects of aspect ratio and cross-sectional shape on the wake structure behind a cantilever." ARPN J. of Eng. and App. Sci. 11 (2016).

[19] Okamoto, T., and M. Yagita. "The experimental investigation on the flow past a circular cylinder of finite length placed normal to the plane surface in a uniform stream." *Bulletin of JSME* 16, no. 95 (1973): 805-814.

[20] Park, C. W., and S. J. Lee. "Free end effects on the near wake flow structure behind a finite circular cylinder." *Journal of Wind Engineering and Industrial Aerodynamics* 88, no. 2 (2000): 231-246.

[21] Tian, F. B., H. Dai, H. Luo, J. F. Doyle, and B. Rousseau. "Fluid–structure interaction involving large deformations: 3D simulations and applications to biological systems." *Journal of computational physics* 258 (2014): 451-469.

[22] Tiong, Y. K., et al. "The Feasibility of Wind and Solar Energy Application for Oil and Gas Offshore Platform." *IOP Conference Series: Materials Science and Engineering*. Vol. 78. No. 1. IOP Publishing, 2015.